ELSEVIER

Contents lists available at ScienceDirect

Applied Catalysis B: Environment and Energy

journal homepage: www.elsevier.com/locate/apcatb





Photocatalytic CO₂ reduction to methanol with metal free thiadiazole-based covalent organic frameworks

Yu-Chen Wang ^a, Wen-Jie Shi ^{a,*} , Wei-Xue Tao ^a, Yun Su ^c, Xiang-Yang Wang ^b, Cheng Wang ^b, Di-Chang Zhong ^{a,*}, Tong-Bu Lu ^{a,*}

- a Institute for New Energy Materials and Low Carbon Technologies, School of Materials Science and Engineering, Tianjin University of Technology, Tianjin 300384, China
- ^b College of Chemistry and Chemical Engineering, iCHEM, PCOSS Xiamen University, Xiamen 361005, China
- ^c School of Environmental Science and Safety Engineering, Tianjin University of Technology, Tianjin 300384, China

ARTICLE INFO

Keywords:
Covalent organic frameworks
Metal-free catalyst
Photocatalysis
CO₂ reduction
Polarization effect

ABSTRACT

Photocatalytic CO_2 reduction into methanol offers a sustainable method for methanol production. However, the current catalytic efficiency remains insufficient to meet the scale requirements. One of the effective strategies for enhancing catalytic efficiency is to accelerate the electron separation and transfer. Herein, we constructed a thiadiazole-based covalent organic frameworks (COFs) functionalized with cyclohexanetrione group. The cyclohexanetrione group is conducive to the charge separation and transfer processes via the polarization effect. As a result, this COF shows outstanding photocatalytic activity for CO_2 reduction to methanol, with a methanol yield reaching as high as 27.74 mmol/g/h and a remarkable quantum efficiency up to 7.39 % at 450 nm. These values are much higher than those of the counterpart without cyclohexanetrione group, and represent the best catalytic activity in photocatalytic CO_2 reduction to methanol among reported catalysts. This work has revealed the polarization effect in boosting CO_2 reduction at the molecular level, giving new insights in developing efficient photocatalysts for CO_2 reduction.

1. Introduction

Methanol (CH₃OH) holds a crucial role in modern chemical industry due to its versatility (Scheme 1a) [1–4]. In industry, the CH₃OH production is usually achieved by CO₂ hydrogenation process, where the main challenge is the high energy consumption due to the requirements of high temperature and pressure [5–7]. Photocatalytic CO₂ reduction reaction (CO₂RR) [8–10] offers a mild and sustainable approach for CH₃OH production (Scheme 1b). Since the process of CO₂ reduction to CH₃OH undergoes multi-steps of electron and proton transfer (CO₂ + 6 H⁺ + 6e $^-$ CH₃OH + H₂O; -0.38 V vs. NHE) [11–14], it is a huge challenge to efficiently promote the 6e $^-$ CO₂RR. Accelerating electron transfer can boost the reaction kinetics of the 6e $^-$ CO₂RR to CH₃OH, it is critical to rationally design and synthesize photocatalysts featuring fast electron transfer rate.

Recently, many metal-based photocatalysts have been developed to promote the $6e^-$ CO₂RR to CH₃OH [15–17]. In contrast, the metal-free photocatalysts for the $6e^-$ CO₂RR to CH₃OH were reported limitedly. Covalent organic frameworks (COFs), as a type of metal-free

molecule-based crystalline porous materials, have attracted considerable interest in photocatalytic CO_2 reduction [18–20]. Their high stability and modifiable architectures enable them not only to favor for the introduction of light-absorbing moieties, but also allow for precisely regulating functional group of the catalysts [21–26]. Lan and Ye groups have respectively adjusted the balance between electron-deficient and electron-rich components within the monomers, achieving significant breakthrough in photocatalytic CO_2 -to-HCOOH/CO conversion [27,28]. Despite these advances, the efficient production of CH_3OH from CO_2 reduction using metal-free COF_3 remains an understudied area, which may mark the development of photocatalytic conversion technology in this field.

Addressing this gap necessitates COF design transcending traditional limitations, enabling the efficient and mild-condition conversion of $\rm CO_2$ to $\rm CH_3OH$. Given these considerations, we proposed that incorporation of the cyclohexanetrione functional group onto thiadiazole-based covalent organic frameworks to get high-efficiency COFs photocatalysts for $\rm CO_2$ reduction. Firstly, the thiadiazole unit is a light-absorbing moiety, the incorporation of which would reduce the dependence on

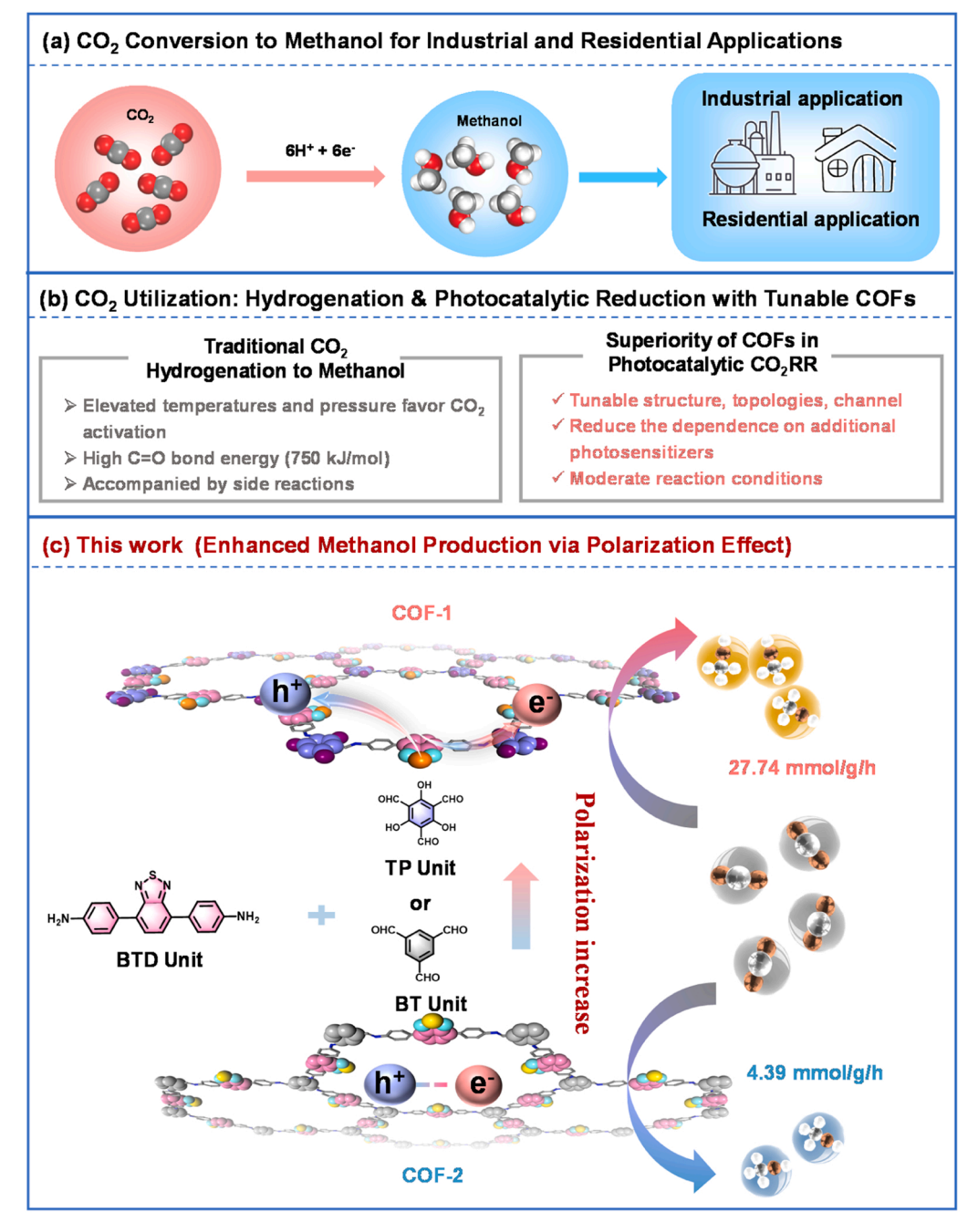
E-mail addresses: wjshi@email.tjut.edu.cn (W.-J. Shi), dczhong@email.tjut.edu.cn (D.-C. Zhong), lutongbu@tjut.edu.cn (T.-B. Lu).

^{*} Corresponding authors.

additional photosensitizers. Secondly, the implementation of cyclohexanetrione functional group through polarization engineering will significantly enhance the electron-hole separation efficiency in COFs. This modification imparts unique electronic properties at the molecular level to thiadiazole-based COFs, thereby may optimize the photocatalytic ${\rm CO_2}$ reduction performance.

Based on the above consideration, we functionalized a thiadiazole-based COF with cyclohexanetrione moiety (COF-1). This modulation really enhances the built-in electric field of thiadiazole-based COF. As expected, COF-1 exhibits outstanding photocatalytic activity for $\rm CO_2$ reduction to CH₃OH, achieving an unprecedented yield of 27.74 mmol/g/h, which is much higher than that of the counterpart without cyclohexanetrione (COF-2, 4.39 mmol/g/h, Scheme 1c). Upon excitation at

395, 450 and 530 nm, the apparent quantum yield (AQY) reach as high as 9.45 %, 7.39 % and 6.99 %, respectively. Density functional theory (DFT) calculations indicated that the introduction of cyclohexanetrione moiety significantly enhances polarization in COF-1, resulting in ca. 150 %-fold increase in the dipole. The results of ultrafast transient absorption (TA) experiments further reveal that the cyclohexanetrione moiety is beneficial for the charge separation and transfer processes. This study unravels that the polarization in catalysts is beneficial for boosting photochemical CO_2 reduction, which will pave a new way for development of efficient COF photocatalysts.



Scheme 1. (a) CO_2 conversion to methanol for industrial and residential applications. (b) Comparative analysis of traditional CO_2 hydrogenation and COFs in photocatalytic CO_2 reduction to methanol. (c) Schematic diagram showing the syntheses of COF-1 and COF-2, as well as their photocatalytic performance for CO_2 reduction to CH_3OH .

2. Experimental methods

2.1. Synthesis of COF-1

4,4'-(benzo[c][1,2,5]thiadiazole-4,7-diyl)dianiline (BTD, 5.96 mg, 0.0187 mmol, 3 equiv.) and 2,4,6-trihydroxybenzene-1,3,5-tricarbaldehyde (TP, 2.47 mg, 0.0125 mmol, 2 equiv.) were added to the solution of o-dichlorobenzene/n-butyl alcohol ($\nu/\nu=1/1$, 2 mL) in a 10 mL Pyrex tube. The orange mixture was sonicated for 20 min, 3 M acetic acid (0.1 mL) was added. Then, the tube was frozen in the liquid N₂ bath at 77 K and degassed by three freeze-pump-thaw cycles. Afterwards, the tube was kept at 120 °C for three days. After cooling to room temperature, the red precipitate was collected by filtration and washed with THF. To remove the monomer completely, the precipitate was washed several times with THF and centrifuged, until supernatant became colorless. Finally, the precipitate was dried under vacuum overnight, yielding bright red powder.

2.2. Synthesis of COF-2

The preparation and treatment of COF-2 was similar to those of COF-1, except that 2,4,6-trihydroxybenzene-1,3,5-tricarbaldehyde (TP) was replaced with benzene-1,3,5-tricarbaldehyde (BT, 2.03 mg, 0.01253 mmol, 2 equiv.), yielding red-orange powder.

2.3. Photocatalytic experiment

The photocatalytic CO_2 reduction was conducted in a 17 mL quartz vessel containing COF (1 mg) as catalyst, TEOA (300 μ L) as electron donor in 5 mL CH₃CN/H₂O ($\nu/\nu=4:1$) solvents at 298 K. After purging the system with CO_2 for 25 min to remove O_2 and other gases, the photocatalytic reaction was initiated by irradiation under a 300 W Xe lamp (100 mW/cm²). The liquid products possibly formed were analyzed by headspace gas chromatography (HS-GC) and ion chromatography (IC), and the possible gas products were analyzed by gas chromatography. Each photocatalytic reaction was repeated at least three times to confirm the reliability of the data. Recycling experiments were carried out under similar conditions by using the collected catalyst after photocatalytic test instead of fresh catalyst.

3. Results and discussion

3.1. Syntheses and characterization

COF-1 and COF-2 were synthesized via Schiff-base condensation reactions of 4,4'-(benzo[c][1,2,5]thiadiazole-4,7-diyl)dianiline (BTD) with 2,4,6-trihydroxybenzene-1,3,5-tricarbaldehyde (TP) and 1,3,5-benzenetricarboxaldehyde (BT), respectively (Scheme 1 and Scheme S1). The experimental powder X-ray diffraction (PXRD) patterns are

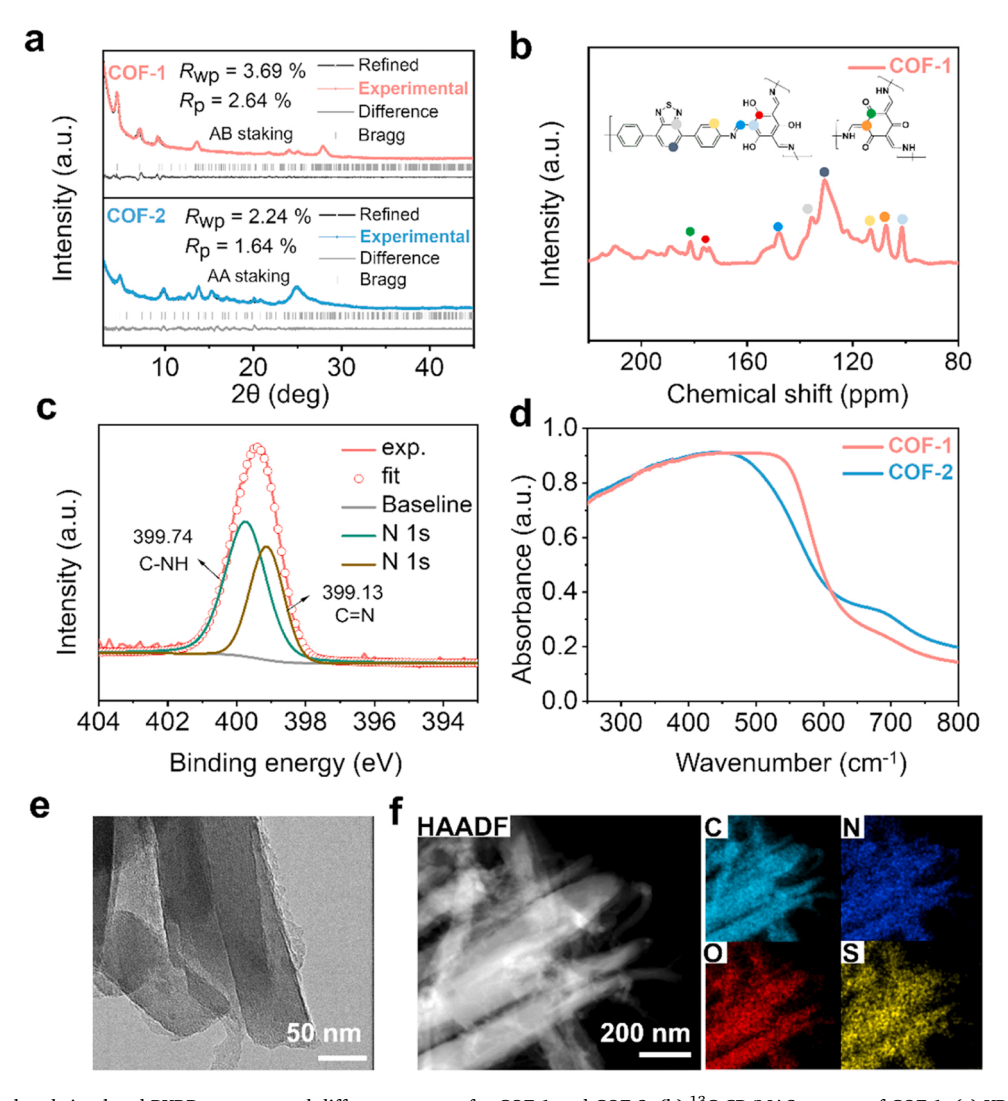


Fig. 1. (a) Experimental and simulated PXRD patterns and difference curves for COF-1 and COF-2. (b) ¹³C CP/MAS spectra of COF-1. (c) XPS deconvoluted N1s of COF-1. (d) UV-Vis DRS of COF-1 and COF-2. (e) TEM image of COF-1. (f) HAADF-STEM image and corresponding element mapping of COF-1.

consistent with the simulated patterns, confirming the crystallinity and the successful syntheses of both COFs (Fig. 1a). By further Pawley refinement, the single-cell parameters were obtained as a = $b = 38.27 \text{ Å}, c = 6.60 \text{ Å}, R_{\text{wp}} = 3.69 \text{ %}$ and $R_{\text{p}} = 2.64 \text{ %}$ for COF-1, and $a = b = 37.53 \text{ Å}, c = 3.52 \text{ Å}, R_{WD} = 2.24 \% \text{ and } R_{D} = 1.64 \% \text{ for COF-2}.$ Fourier transform infrared (FT-IR) spectroscopy revealed a distinctive peak at 1621–1627 cm⁻¹ for both COF-1 and COF-2, which can be assigned to the C=N stretching vibration (Figs. S1 and S2), proving the success of polymerization. Solid-state NMR (NMR) spectroscopy further showcased a signal at ~150 ppm for the -C=N bond (Fig. 1b and Fig. S3). Moreover, a distinct signal for the C-OH bond at \sim 176 ppm was appeared for COF-1 [29]. In addition, the X-ray photoelectron spectroscopy (XPS) of COF-1 showed that the N 1 s spectrum presented peaks at 399.74 and 399.13 eV, corresponding to C-NH and C=N groups, respectively (Fig. 1c). The O 1 s spectrum showed two peaks at 531.61 and 533.24 eV, attributing to C=O and C-OH bond (Fig. S4). These results reveal that the O atoms are in both the enol and keto forms in COF-1 [30]. In the S 2p spectra, two main characteristic binding energy peaks at 165.26 and 166.42 eV are found, belonging to S2p_{3/2} and S2p_{1/2} (Fig. S5). In contrast to COF-1, the co-existence of N, C, and S were confirmed in COF-2 via XPS analysis (Figs. S6-S8), with the N1s

spectra highlighting a peak at 399.05 eV for the C=N bond (Fig. S6). UV-Vis diffuse reflectance spectroscopy (DRS) revealed similar light absorption profiles for both COFs (Fig. 1d and Figs. S9-S10). High-resolution scanning electron microscopy (HR-SEM) and transmission electron microscopy (TEM) images revealed rod-like morphologies for both COFs (Fig. 1e and Figs. S11-S15). Energy-dispersive X-ray (EDX) element mapping demonstrated the uniform distribution of C, N, O, and S in COF-1 and C, N, and S in COF-2, highlighting the elemental homogeneity within the frameworks (Fig. 1f and Fig. S16). The contact angle measurements unveiled the pronounced hydrophilic surfaces of COF-1, as evidenced by contact angle of 54.49°, while COF-2 possesses less hydrophilic surface with bigger contact angle of 101.73° (Fig. S17). Thermogravimetric (TG) analyses affirmed that both COFs possess good thermal stability (Fig. S18). The Brunauer-Emmett-Teller (BET) analysis showed that the surface areas of COF-1 and COF-2 are 212.05 and 192.76 m²/g, respectively, and the average pore sizes are 1.46 and 1.66 nm, respectively (Figs. S19-S22). COF-1 demonstrated a superior CO₂ adsorption capacity of 14.35 cm³ g⁻¹ compared with COF-2 (Fig. S23).

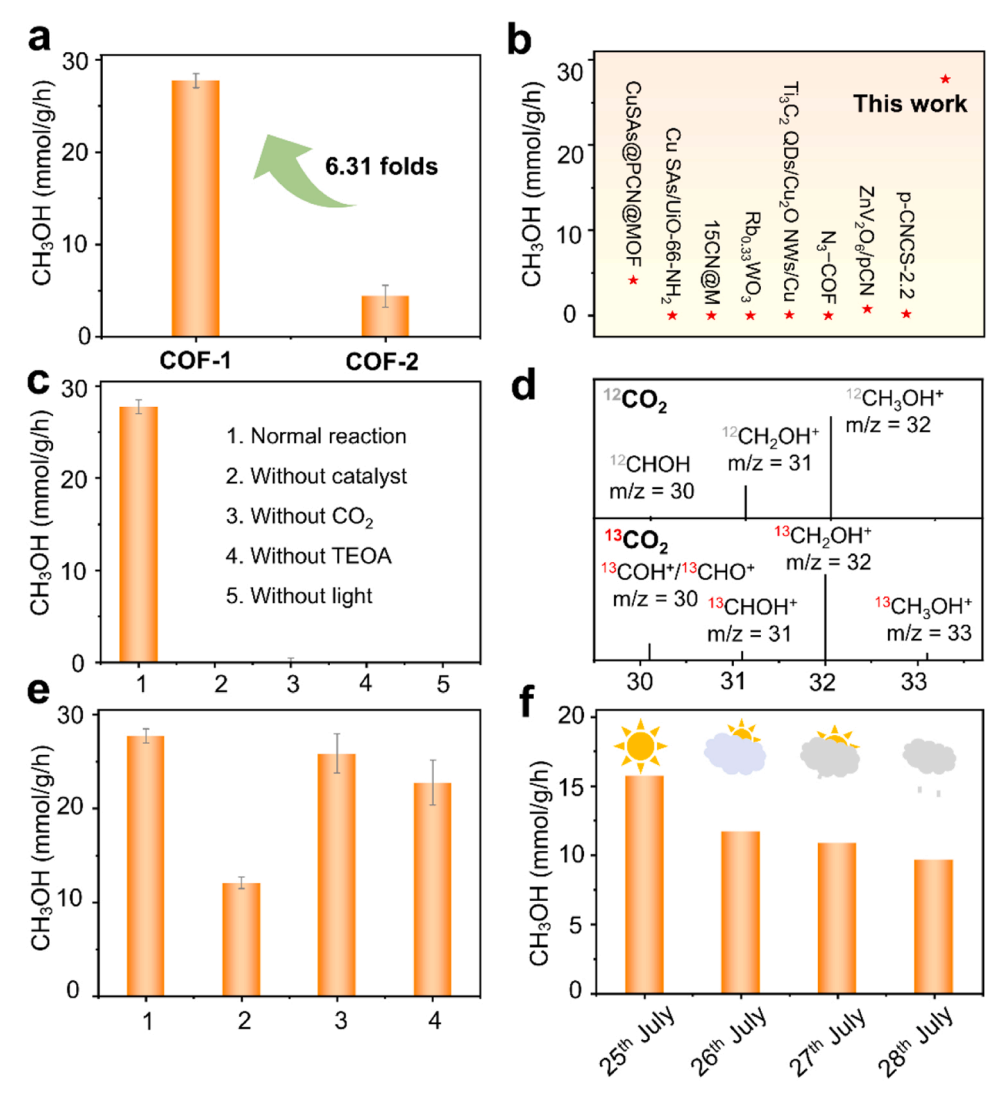


Fig. 2. (a) CH₃OH production rates of COF-1 and COF-2 in photocatalytic CO₂RR. (b) CH₃OH production rates of COF-1 and reported typical catalysts in CO₂RR. (c) Control experiments of photocatalytic CO₂ reduction by COF-1. (d) MS chromatograms of the liquid products of photocatalytic 12 CO₂/ 13 CO₂ reduction by COF-1. (e) Photocatalytic CH₃OH production by COF-1 under different gas environments. 1. 100 % CO₂ in lab; 2. 10 % CO₂ in lab; 3. CO₂ from DCM waste (~100 %); 4. CO₂ from DCM waste (~70 %). (f) Photocatalytic CH₃OH production under natural sunlight (from 25th to 28th July 2023). Normal reaction conditions: Catalyst (1 mg), TEOA (300 μL), CH₃CN/H₂O (ν/ν = 4:1; 5 mL), 300 W Xe lamp, 10 h, 25 °C.

3.2. Photocatalytic properties

The photocatalytic CO2 reduction by COF-1 and COF-2 were performed in a 17.5 mL glass tube at room temperature, containing COF as the photocatalyst and triethanolamine (TEOA) as the sacrificial reductant in a mixture of 5 mL CO2-saturated CH3CN/H2O solution. The mixture was bubbled with CO2 for 25 min and then irradiated under a 300 W Xe lamp. The gaseous products were detected by gas chromatography, and the liquid products were examined by headspace gas chromatography (HS-GC) and ion chromatography (IC). The results show that no gas-phase detected and CH₃OH was the primary product, and a trace amount of HCOOH was detected. When the amount of TEOA was 300 µL, COF-1 achieves optimal performance (Fig. S24). Under a 100 % CO₂ atmosphere, the CH₃OH production rate for COF-1 reaches as high as 27.74 mmol/g/h, 6.31 times higher than COF-2 (4.39 mmol/ g/h) (Fig. 2a and Fig. S25). This value is highest among reported pristine COF photocatalysts (Table S1) and other photocatalysts (Fig. 2b) [31-40]. The investigation on wavelength-dependent apparent quantum yield (AOY) shows that the AOY of COF-1 for CO2 reduction reach as high as 9.45, 7.39 and 6.99 % at 395, 450 and 530 nm, respectively (Fig. S26). To identify the key factors for CO2 reduction, a series of control experiments were carried out over COF-1. As shown in Fig. 2c, no CH3OH can be detected in the lack of COF-1, TEOA, CO2 or light, illustrating that all these components are indispensable to CO2 photoreduction. To conclusively determine the carbon source in the generated CH₃OH, isotopic tracing experiment was conducted. As shown in Fig. 2d, the liquid products of photocatalytic ¹²CO₂ reduction by COF-1 show m/z signals at 30, 31 and 32, which can be assigned to ¹²CHOH, ¹²CH₂OH⁺ and ¹²CH₃OH⁺, respectively. After replacing ¹²CO₂ with $^{13}\text{CO}_2$, the m/z signals at 30, 31, 32 and 33 appeared, which can be attributed to ¹³COH⁺/¹³CHO⁺, ¹³CHOH⁺, ¹³CH₂OH⁺ and ¹³CH₃OH⁺. These results solidly confirm that the produced CH₃OH originates from the CO_2 reduction [14].

The high activity of COF-1 for photocatalytic CO2 reduction was further evaluated under simulated flue gas containing 10 % CO2 (CO2/ Ar = 10/90; ν/ν). Noteworthy that COF-1 still demonstrated a CH₃OH yield of 12.09 mmol/g/h, indicating the high catalytic efficiency of COF-1 in lower CO₂ concentration. To further test the toxicity resistance of COF-1, we transformed the prevalent industrial byproduct CO2 derived from the industrial dichloromethane (DCM) waste into the catalytic system (Fig. S27). As shown in Fig. 2e, COF-1 also possesses excellent activity for photocatalytic reduction of CO2 waste gas to CH₃OH, with CH₃OH yield rate of 25.89 (~100 % CO₂ from DCM waste) and 22.77 mmol/g/h (~70 % CO₂ from DCM waste), respectively, which solidly confirmed the high activity of COF-1 in photocatalytic CO₂ reduction. Furthermore, the catalytic activity of COF-1 for CO2 reduction was also investigated under natural sunlight (Fig. S28). As shown in Fig. 2f, COF-1 show photocatalytic activity for CO₂ reduction to CH₃OH under variable weather conditions. Even under simulated flue gas containing 10 % CO₂, COF-1 showed a CH₃OH production rate of 7.41 mmol/g/h upon natural sunlight irradiation on 22nd September 2023 (Fig. S29). These observations confirm that COF-1 really possesses excellent photocatalytic activity for CO2 reduction to CH3OH.

The durability of COF-1 for photocatalytic CO_2 reduction was further tested. As displayed in Fig. S30, the catalytic performance of COF-1 showed no notable decrease in CH_3OH production rates after three runs of photocatalytic CO_2 reduction, which proves the good stability of COF-1. In addition, PXRD, IR spectroscopy, and TEM (Figs. S31-S33) further confirmed the structural and compositional integrity of COF-1 after photocatalysis. Similarly, COF-2 also demonstrated good stability in photocatalytic CO_2 reduction reaction, as convinced by PXRD, IR, and TEM (Figs. S34-S36).

3.3. Photoelectrochemical property

The photogenerated charge separation and transfer of COF-1 and

COF-2 were further investigated by photocurrent response, electrochemical impedance spectroscopy (EIS), transient absorption spectroscopy (TAS), steady-state and time-resolved photoluminescence (PL and TRPL, respectively) spectroscopies. Photocurrent tests revealed a pronounced enhancement in photocurrent generation by COF-1 under illumination compared with COF-2 (Fig. S37), indicating a more efficient charge separation and transfer in COF-1, which was further proved by EIS results, where a smaller diameter of capacitive loop for COF-1 than COF-2 was observed (Fig. S38). Upon excitation at 450 nm, COF-1 exhibited a substantially reduced and redshifted emission, as well as decreased charge carrier lifetimes ($\tau_{ave} = 0.43 \text{ ns}$) in contrast to COF-2 ($\tau_{\rm ave} = 0.69 \, {\rm ns}$), also indicating the more effective charge separation and transfer of COF-1 over COF-2 (Figs. S39 and S40). To gain further insight into the rapid charge separation of COF-1, the ultrafast transient absorption (TA) spectroscopy was conducted (Fig. 3a and Fig. S41). Under pumping light excitation at $\lambda = 380$ nm, both COF-1 and COF-2 show an apparent ground-state bleaching (GSB) signal at ~513 nm. By fitting the excited state kinetics at 580 and 650 nm (Figs. 3b and c; Tables S2-S3), the decay times can be obtained in COF-1 were < 1 ps, \sim 64 ps, and \sim 1.5 ns, and those of COF-2 were \sim 3 ps, \sim 40 ps, and 0.81 ns, respectively. It can be observed that COF-1 shows the shorter decay time compared to that of COF-2 in charge separation process (< 1 ps) and longer decay time (~1.5 ns) compared to that of COF-2 in charge recombination process [41,42]. These results suggest that the cyclohexanetrione moiety in COF-1 effectively accelerates the charge separation and averts the charge recombination [43,44].

To theoretically reveal the better photocatalytic activity of COF-1 over COF-2, density functional theory (DFT) calculations were performed to evaluate the efficiency of charge separation and transfer in both COFs. The dipole moment of COF-1 was determined to be 30.04 Debye for COF-1, ca. 150 % higher than COF-2 (20.80 Debye). The higher Debye in COF-1 can facilitate in-plane charge transfer [45] and thus enhance the photocatalytic CH₃OH yields for COF-1 (Fig. S42). The natural population analysis (NPA) was employed to assess the impact of integrating the cyclohexanetrione moiety on the in-plane charge transfer. As shown in Fig. 3d, the C1 atom of benzene and S atom of thiadiazole ring in COF-1 exhibits a relatively stronger polarization (0.172e and 0.886e, respectively) than COF-2 (0.114e and 0.872e, respectively). This enhancement in electron density in COF-1 is more conducive to the in-plane charge transfer [46–48].

To gain deeper insights into the spatial distribution of electron-hole of COF-1 and COF-2, the time-dependent density functional theory (TD-DFT) calculations and electron-hole excitation analyses were carried out (Figs. S43-S51 and Tables S4-S8). All transition densities of the 50 excited states (ES) were calculated. By comparing the action spectra with the simulated energy spectra, the possible excited states contributing to the $\rm CO_2RR$ are predicted as ES3 and ES4 for COF-1 and COF-2 (Fig. 3e and Tables S4-S5), where the photogenerated electrons and holes are highlighted in the population analysis (Figs. S46 and S47; Figs. S50 and S51). Compare with COF-2, COF-1 exhibits a higher electrons and holes distribution density of ES. These results suggest that introduction of polar moieties can promote electron-hole accumulation during photoexcitation at the thiadiazole unit and cyclohexanetrione moiety.

Additionally, the distances (D index) between electron and hole centers, the hole delocalization index (HDI) and electron delocalization index (EDI) were utilized to examine the density of departure states for photo-generated electrons and holes in COF-1 and COF-2 (Fig. 3f and Tables S6-S7) [49–52]. It is noteworthy that compared with COF-2, the D index value in ES3 and ES4 of COF-1 undergoes a sharp increase, and the intensities of EDI increase from 4.53 to 6.12 in ES3 and 4.48 to 5.97 in ES4. Similarly, the HDI value rises from 4.87 to 7.10 in ES3 and 4.86 to 7.57 in ES4. These increases suggest that the concentration of electrons and holes were higher in COF-1, which greatly contributes to the enhanced $\rm CO_2$ reduction kinetics [53].

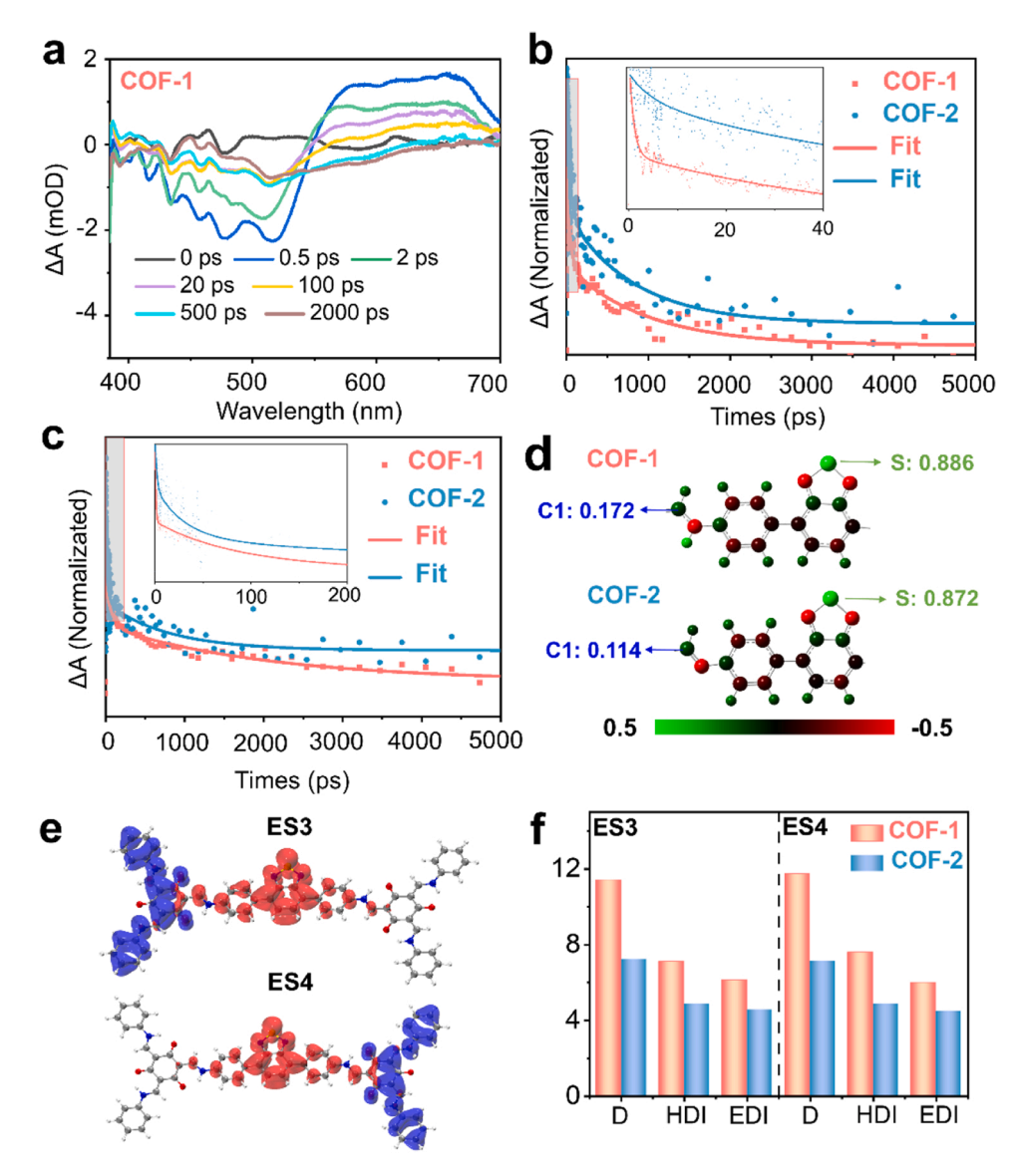


Fig. 3. (a) TA spectra of COF-1 using a pump with the wavelength of 380 nm. (b) Kinetic parameters of photophysical data at 580 nm from TA spectra. (c) Kinetic parameters of photophysical data at 650 nm from TA spectra. (d) Illustration of the charge distribution of COF-1 and COF-2 from TD-DFT calculations. (e) Population of electron and hole distributions (ES3 and ES4) of COF-1 obtained by TD-DFT. (f) The D index, HDI and EDI of ES3 and ES4 for COF-1 and COF-2.

3.4. Photocatalytic reaction mechanism

Tauc plots were analyzed for COF-1 and COF-2, revealing the band gaps (Eg) to be 1.87 and 1.82 eV ν s. NHE, respectively (Figs. S52 and S53). By Mott Schottky plots (Figs. S54 and S55), the flat band position (V_{fb}) was determined to be -1.25 eV (COF-1), -1.12 eV (COF-2) ν s. NHE, respectively. These values correspond to the lowest unoccupied molecular orbital (LUMO). Combined with the results of band gaps, the highest occupied molecular orbital (HOMO) of COF-1 and COF-2 were calculated to be 0.62 and 0.70 eV ν s. NHE, respectively. Based on these findings, the energy-band alignments of both COF-1 and COF-2 are presented in Fig. 4a. It is noteworthy that the LUMO potentials of both COF-1 and COF-2 are more negative than the redox potential for the CO₂ reduction to CH₃OH (-0.38 V ν s. NHE), indicating their theoretical capacity to serve as catalysts for CO₂ reduction to CH₃OH.

To determine the catalytic center for $\rm CO_2$ reduction, XPS measurements of COF-1 were conducted before and after irradiation. As depicted in Fig. S56, the N1s binding energies of COF-1 locate at 399.13 and 399.74 eV in the dark, which shows negative shift to 399.00 and 399.61 eV respectively upon light irradiation, indicating that the N site

in the imine group accepts electron and may serve as the catalytic center. In addition, no significant binding energy shift observed in S and C upon light irradiation further supports the results (Fig. S57 and S58). Given that the reduction of CO2 to CH3OH can proceed via two possible pathways with different *COOH/*CO and HCOO* intermediates, we conducted experiments to verify the dominant pathway. Specifically, carbon monoxide (CO) and formic acid (HCOOH) were directly introduced into the reaction system, respectively. As the addition of HCOOH into the catalysis system resulted in a notably enhanced CH₃OH yield of 36.93 mmol/g/h (Fig. 4b), indicating the HCOO* is the mainly intermediate in the process of CO2 conversion to CH3OH. Conversely, the direct introduction of CO into the system yielded a lower CH₃OH production rate of 5.19 mmol/g/h, also in turn suggesting that the predominant pathway for CH3OH production through the HCOO* intermediate. In addition, the detection of HCOOH in the liquid-phase products provides additional evidence to support this finding (Fig. S59). This result was further supported by in situ FT-IR spectra upon illumination. As depicted in Fig. 4c, the in situ FT-IR spectra of COF-1 exhibited distinct absorption peaks at 1645 cm⁻¹, corresponding to the vibrational modes of HCOO* [54]. Additionally, the HCO*, a key

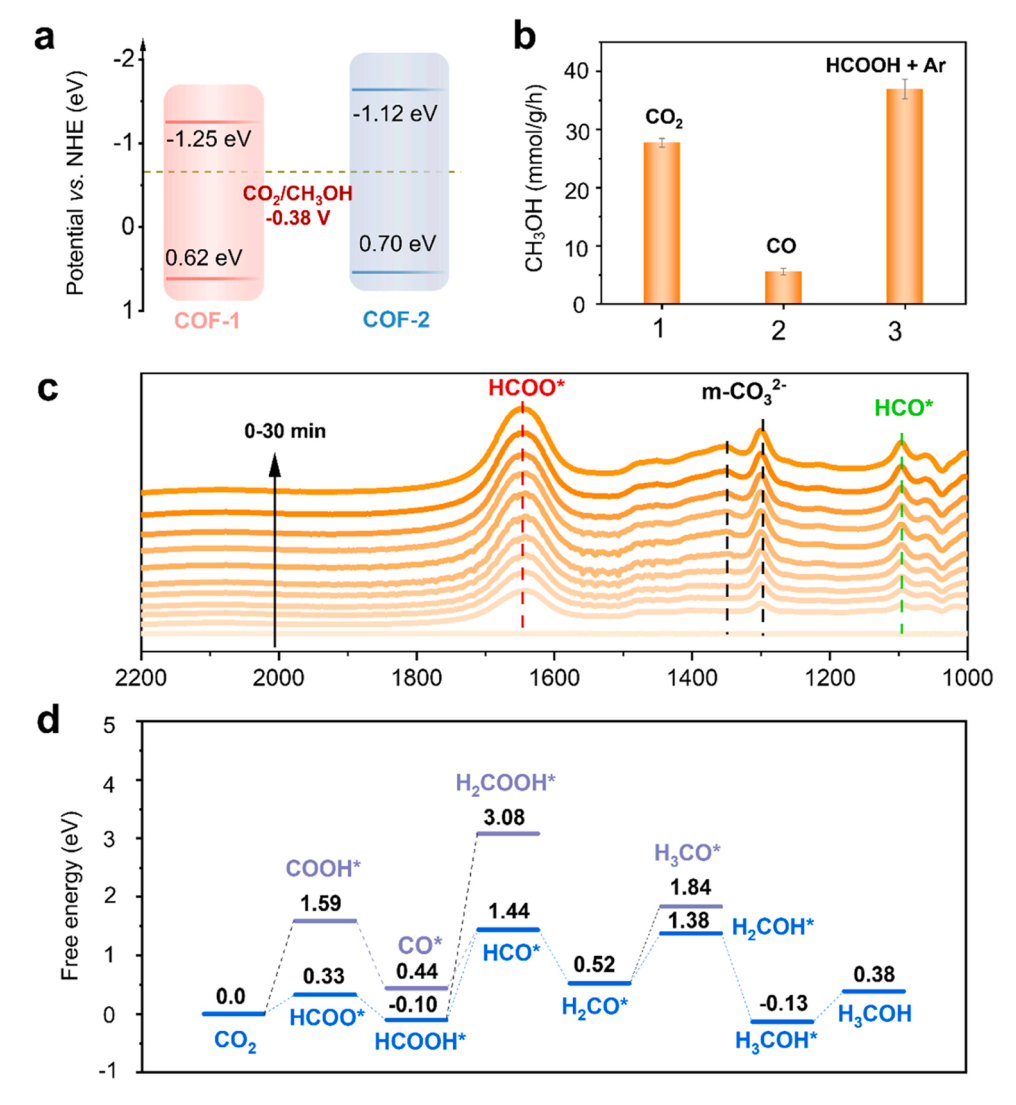


Fig. 4. (a) Energy structures of COF-1 and COF-2. (b) Photocatalytic activity of COF-1 by using CO₂, CO or HCOOH as the reactant (1. CO₂; 2. CO; 3. HCOOH + Ar). (c) FT-IR spectra of COF-1 in the photocatalytic CO₂RR. (d) Calculated free energy diagram of all intermediates for CO₂ reduction to CH₃OH by COF-1.

intermediate during the CO_2 reduction to CH_3OH was also observed, with a characteristic peak at 1095 cm^{-1} [55].

DFT calculations on the Gibbs free energy (ΔG) diagrams were further performed to reveal the reaction thermodynamics. The relative ΔG profile (Fig. 4d and Fig. S60) was constructed at the B3LYP-D3/ 6-311*G(d) level, considering the reaction intermediates perceived from FT-IR analysis. Initially, under irradiation, photogenerated electron transfer to N in the imine group, which facilitates CO₂ adsorption and hydrogenation, leading to the formation of HCOO* intermediate (Figs. S57 and S58), since HCOO* formation ($\Delta G = 0.33$ eV) is kinetically more favorable than COOH* ($\Delta G = 1.59 \text{ eV}$). Based on DFT calculation results, the HCOO* intermediate is easily converted into HCOOH* ($\Delta G = -0.43$ eV). Subsequently, through a proton-coupled electron transfer (PCET) step, the C-O bond cleavage was facilitated, resulting in the formation of the HCO* intermediate. Importantly, the formation of HCO* emerges as the rate-determining step (RDS) with a notable free energy change ($\Delta G = 1.54$ eV for COF-1). After three PCET processes, the finial product CH₃OH was released via H₂CO*, H₂COH* and H_3COH^* intermediates. A comparative analysis between COF-1 and COF-2 in RDS step reveals that COF-1 presents lower energy barriers $(\Delta G = 1.54 \text{ eV versus } \Delta G = 1.71 \text{ eV for COF-2})$, indicating a more favorable process of CO₂ reduction to CH₃OH by COF-1 over COF-2.

4. Conclusions

In summary, we have rationally designed and synthesized a thiadiazole-based COF functionalized with polar cyclohexanetrione moiety, which shows significantly improved photocatalytic activity for $\rm CO_2$ reduction to $\rm CH_3OH$. The incorporation of cyclohexanetrione moiety onto thiadiazole-based COF enhances polarization, leading to a significant promotion of charge separation, therefore collectively promoting the photosynthesis of $\rm CH_3OH$. Specifically, this COF presents a $\rm CH_3OH$ production yield of 27.74 mmol/g/h in photocatalytic $\rm CO_2$ reduction, which is 6.31-folds higher than that without cyclohexanetrione moiety. Even in $\rm CO_2$ waste gas (~ 70 % $\rm CO_2$ from DCM waste), $\rm COF-1$ still exhibit excellent photocatalytic performance for $\rm CO_2$ reduction to $\rm CH_3OH$, with a high production rate of 22.77 mmol/g/h. The results in this work pave a new way for researchers in designing high performance metal-free COFs photocatalysts for $\rm CO_2$ reduction.

CRediT authorship contribution statement

Yu-Chen Wang: Writing-original draft, Methodology, Investigation. Wen-Jie Shi: Writing-review & editing, Supervision, Methodology. Wei-Xue Tao: Investigation. Yun Su: Investigation. Xiang-Yang Wang: Investigation. Cheng Wang: Investigation. Di-Chang Zhong: Writing-

review & editing, Supervision, Methodology, Funding acquisition, Conceptualization. Tong-Bu Lu: Supervision.

Declaration of Competing Interest

The authors declare that they have no known competing financial interests or personal relationships that could have appeared to influence the work reported in this paper.

Acknowledgments

This work was supported by the National Key R&D Program of China (2022YFA1502902), the National Natural Science Foundation of China (22201209, 22271218, 22071182, and 21931007).

Appendix A. Supporting information

Supplementary data associated with this article can be found in the online version at doi:10.1016/j.apcatb.2025.125404.

Data availability

No data was used for the research described in the article.

References

- [1] X. Jiang, X.-W. Nie, X.-W. Guo, C.-S. Song, J.-G. Chen, Recent advances in carbon dioxide hydrogenation to methanol via heterogeneous catalysis, Chem. Rev. 120 (2020) 7984–8034.
- [2] I. Yarulina, A.-D. Chowdhury, F. Meirer, B.-M. Weckhuysen, J. Gason, Recent trends and fundamental insights in the methanol-to-hydrocarbons process, Nat. Catal. 1 (2018) 398–411.
- [3] A.-A. Tountas, G.-A. Ozin, M.-M. Sain, Solar methanol energy storage, Nat. Catal. 4 (2021) 934–942.
- [4] S. Navarro-Jaén, M. Virginie, J. Bonin, M. Robert, R. Wojcieszak, A. Khodakov, Highlights and challenges in the selective reduction of carbon dioxide to methanol, Nat. Rev. Chem. 5 (2021) 564–579.
- [5] N. Onishi, Y. Himeda, Homogeneous catalysts for CO₂ hydrogenation to methanol and methanol dehydrogenation to hydrogen generation, Coord. Chem. Rev. 472 (2022) 214767.
- [6] F. Studt, I. Sharafutdinov, F. Abild-Pedersen, C.-F. Elkjær, J.-S. Hummelshøj, S. Dahl, I. Chorkendorff, J.-K. Nørskov, Discovery of a Ni-Ga catalyst for carbon dioxide reduction to methanol, Nat. Chem. 6 (2014) 320–324.
- [7] H. Wang, H.-F. Qi, X. Sun, S.-Y. Jia, X.-Y. Li, T.-J. Miao, L.-Q. Xiong, S.-H. Wang, X.-L. Zhang, X.-Y. Liu, A.-Q. Wang, T. Zhang, W.-X. Huang, J.-W. Tang, High quantum efficiency of hydrogen production from methanol aqueous solution with PtCu-TiO₂ photocatalysts, Nat. Mater. 22 (2023) 619–626.
- [8] J. Xie, Z.-J. Lu, Y. Feng, J.G. Huang, J.D. Hu, A.-Z. Hao, Y.-L. Cao, A small organic molecule strategy for remedying oxygen vacancies by bismuth defects in BiOBr nanosheet with excellent photocatalytic CO₂ reduction, Nano Res. 17 (2024) 297–306.
- [9] Y.-D. Zhang, Y.-J. Sun, Q.-Y. Wang, Z.-C. Zhuang, Z.-T. Ma, L.-M. Liu, G.-M. Wang, D.-S. Wang, X.-S. Zheng, Synergy of photogenerated electrons and holes toward efficient photocatalytic urea synthesis from CO₂ and N₂, Angew. Chem. Int. Ed. 63 (2024) e202405637.
- [10] W.-Y. Pan, Z.-H. Wei, Y.-H. Su, Y.-B. Lian, Z.-Y. Zheng, H.-H. Yuan, Y.-Z. Qin, X.-L. Xie, Q.-Q. Bai, Z.-Y. Jiao, W. Hua, J.-Z. Chen, W.-J. Yang, Z. Deng, Y. Peng, Hydroxylated metal-organic-layer nanocages anchoring single atomic cobalt sites for robust photocatalytic CO₂ reduction, Nano Res. 17 (2023) 2410–2419.
- [11] N.-Y. Huang, B. Li, D. Wu, Z.-Y. Chen, B. Shao, D. Chen, Y.-T. Zheng, W. Wang, C. Yang, M. Gu, L. Li, Q. Xu, Crystal engineering of MOF-derived bimetallic oxide solid solution anchored with Au nanoparticles for photocatalytic CO₂ reduction to syngas and C₂ hydrocarbons, Angew. Chem. Int. Ed. 63 (2024) e202319177.
- [12] D.-C. Liu, D.-C. Zhong, T.-B. Lu, Non-noble metal-based molecular complexes for CO₂ reduction: from the ligand design perspective, EnergyChem 2 (2020) 100034.
- [13] D.-C. Zhong, Y.-N. Gong, C. Zhang, T.-B. Lu, Dinuclear metal synergistic catalysis for energy conversion, Chem. Soc. Rev. 52 (2023) 3170–3214.
- [14] L.-L. Ling, W.-J. Yang, P. Yan, M. Wang, H.-L. Jiang, Light-assisted CO₂ hydrogenation over Pd₃Cu@UiO-66 promoted by active sites in close proximity, Angew. Chem. Int. Ed. 61 (2022) e202116396.
- [15] A. Li, T. Wang, C.-C. Li, Z.-Q. Huang, Z.-B. Luo, J.-L. Gong, Adjusting the reduction potential of electrons by quantum confinement for selective photoreduction of CO₂ to methanol, Angew. Chem. Int. Ed. 58 (2019) 3804–3808.
- [16] S. Gao, B.-C. Gu, X.-C. Jiao, Y.-F. Sun, X.-L. Zu, F. Yang, W.-G. Zhu, C.-M. Wang, Z.-M. Feng, B.-J. Ye, Y. Xie, Highly efficient and exceptionally durable CO₂ photoreduction to methanol over freestanding defective single-unit-cell bismuth vanadate layers, J. Am. Chem. Soc. 139 (2017) 3438–3445.

- [17] Y.-A. Wu, I. McNulty, C. Liu, K.-C. Lau, Q. Liu, A.-P. Paulikas, C.-J. Sun, Z. Cai, J.-R. Guest, Y. Ren, V. Stamenkovic, L.-A. Curtiss, Y.-Z. Liu, T. Rajh, Facet-dependent active sites of a single Cu₂O particle photocatalyst for CO₂ reduction to methanol, Nat. Energy 4 (2019) 957–968.
- [18] B.-Q. Yu, R.-B. Lin, G. Xu, Z.-H. Fu, H. Wu, W. Zhou, S.-F. Lu, Q.-W. Li, Y.-C. Jin, J.-H. Li, Z.-G. Zhang, H.-L. Wang, Z.-E. Yan, X.-L. Liu, K. Wang, B.-L. Chen, J.-Z. Jiang, Linkage conversions in single-crystalline covalent organic frameworks, Nat. Chem. 16 (2024) 114–121.
- [19] K.-Y. Geng, R.-Y. Liu, S. Dalapati, K.-T. Tan, Z.-P. Li, S.-S. Tao, Y.-F. Gong, Q.-H. Jiang, D.-L. Jiang, Covalent organic frameworks: design, synthesis, and functions, Chem. Rev. 120 (2020) 8814–8933.
- [20] Y.-N. Gong, X.-Y. Guan, H.-L. Jiang, Covalent organic frameworks for photocatalysis: synthesis, structural features, fundamentals and performance, Coord. Chem. Rev. 475 (2023) 214889.
- [21] C.-S. Diercks, O.-M. Yaghi, The atom, the molecule, and the covalent organic framework, Science 355 (2017) eaal1585.
- [22] H. Wang, H. Wang, Z.-W. Wang, L. Tang, G.-M. Zeng, P. Xu, M. Chen, T. Xiong, C.-Y. Zhou, X.-Y. Li, D.-L. Huang, Y. Zhu, Z.-X. Wang, J.-W. Tang, Covalent organic frame-work photocatalysts: structures and applications, Chem. Soc. Rev. 49 (2020) 4135–4165.
- [23] M. Lu, M. Zhang, J. Liu, Y.-F. Chen, J.-P. Liao, M.-Y. Yang, Y.-P. Cai, S.-L. Li, Y.-Q. Lan, Covalent organic framework based functional materials: important catalysts for efficient $\rm CO_2$ utilization, Angew. Chem. Int. Ed. 61 (2022) e202200003.
- [24] Q. Yang, M.-D. Luo, K.-W. Liu, H.-J. Cao, H.-J. Yan, Covalent organic frameworks for photocatalytic applications, Appl. Catal. B Environ. 276 (2020) 119174.
- [25] Y.-R. Wang, H.-M. Ding, X.-Y. Ma, M. Liu, Y.-L. Yang, Y.-F. Chen, S.-L. Li, Y.-Q. Lan, Imparting CO₂ electroreduction auxiliary for integrated morphology tuning and performance boosting in a porphyrin-based covalent organic framework, Angew. Chem. Int. Ed. 61 (2022) e202114648.
- [26] W. Zhou, X. Wang, W.-L. Zhao, N.-J. Lu, D. Cong, Z. Li, P.-G. Han, G.-Q. Ren, L. Sun, C.-C. Liu, W.-Q. Deng, Photocatalytic CO₂ reduction to syngas using metallosalen covalent organic frameworks, Nat. Commun. 14 (2023) 6971.
- [27] M. Zhang, P. Huang, J.-P. Liao, M.-Y. Yang, S.-B. Zhang, Y.-F. Liu, M. Lu, S.-L. Li, Y.-P. Cai, Y.-Q. Lan, Relative local electron density tuning in metal-covalent organic frameworks for boosting CO₂ photoreduction, Angew. Chem. Int. Ed. 62 (2023) e202311999.
- [28] Q.-Q. Tang, Y.-Y. Gu, J. Ning, Y.-K. Yan, L. Shi, M.-S. Zhou, H.-T. Wei, X.-H. Ren, X.-H. Li, J.-X. Wang, C. Tang, L. Hao, J.-H. Ye, Boosting photocatalysis of hydrazone-linked covalent organic frameworks through Introducing electron-rich conjugated aldehyde, Chem. Eng. J. 470 (2023) 144106.
- [29] S. Ghosh, A. Nakada, M.-A. Springer, T. Kawaguchi, K. Suzuki, H. Kaji, I. Baburin, A. Kuc, T. Heine, H. Suzuki, R. Abe, S. Seki, Identification of prime factors to maximize the photocatalytic hydrogen evolution of covalent organic frameworks, J. Am. Chem. Soc. 142 (2020) 9752–9762.
- [30] S.-X. Yang, X. Li, Y. Cheng, W.-W. Fan, X.-J. Lang, L.-Y. Zheng, Q. Cao, Modulating the stacking model of covalent organic framework isomers with different generation efficiencies of reactive oxygen species, ACS Appl. Mater. Interfaces 13 (2021) 29471–29481.
- [31] X.-B. Liu, C.-Y. Zhu, M.-Y. Li, H.-Z. Xing, S.-Y. Zhu, X. Liu, G.-S. Zhu, Confinement synthesis of atomic copper-anchored polymeric carbon nitride in crystalline UiO-66-NH₂ for high-performance CO₂-to-CH₃OH photocatalysis, Angew. Chem. Int. Ed. (2024) e202412408.
- [32] G. Wang, C.-T. He, R. Huang, J.-J. Mao, D.-S. Wang, Y.-D. Li, Photoinduction of Cu single atoms decorated on UiO-66-NH₂ for enhanced photocatalytic reduction of CO₂ to liquid fuels, J. Am. Chem. Soc. 142 (2020) 19339–19345.
- [33] J. Ding, Q.-L. Tang, Y.-H. Fu, Y.-L. Zhang, J.-M. Hu, T. Li, Q. Zhong, M.-H. Fan, H.-H. Kung, Core-shell covalently linked graphitic carbon Nitride-melamine-resorcinol-formaldehyde microsphere polymers for efficient photocatalytic CO₂ reduction to methanol, J. Am. Chem. Soc. 144 (2022) 9576–9585.
- [34] X.-Y. Wu, Y. Li, G.-K. Zhang, H. Chen, J. Li, K. Wang, Y. Pan, Y. Zhao, Y.-F. Sun, Y. Xie, Photocatalytic CO₂ conversion of M_{0.33}WO₃ directly from the air with high selectivity: insight into full spectrum-induced reaction mechanism, J. Am. Chem. Soc. 141 (2019) 5267–5274.
- [35] Z.-P. Zeng, Y.-B. Yan, J. Chen, P. Zan, Q.-H. Tian, P. Chen, Boosting the photocatalytic ability of Cu₂O nanowires for CO₂ conversion by Mxene quantum dots, Adv. Funct. Mater. 29 (2019) 1806500.
- [36] Y.-H. Fu, X.-L. Zhu, L. Huang, X.-C. Zhang, F.-M. Zhang, W.-D. Zhu, Azine-based covalent organic frameworks as metal-free visible light photocatalysts for CO₂ reduction with H₂O, Appl. Catal. B Environ. 239 (2018) 46–51.
- [37] A. Bafaqeer, M. Tahir, N.-A. Amin, Well-designed ZnV₂O₆/g-C₃N₄ 2D/2D nanosheets heterojunction with faster charges separation via pCN as mediator towards enhanced photocatalytic reduction of CO₂ to fuels, Appl. Catal. B Environ. 242 (2019) 312–326.
- [38] A. Li, T. Wang, C.-C. Li, Z.-Q. Huang, Z.-B. Luo, J.-L. Gong, Adjusting the reduction potential of electrons by quantum confinement for selective photoreduction of CO₂ to methanol, Angew. Chem. Int. Ed. 58 (2019) 3804–3808.
- [39] Y.-H. Wang, Y. Liu, L. Tan, X.-H. Lin, Y.-X. Fang, X.-F. Lu, Y.-D. Hou, G.-G. Zhang, S.-B. Wang, Confining ultrafine Pt nanoparticles on In₂O₃ nanotubes for enhanced selective methanol production by CO₂ hydrogenation, J. Mater. Chem. A. 11 (2023) 26804–26811.
- [40] B. Su, M. Zheng, W. Lin, X.-H. Lu, D.-Y. Luan, S.-B. Wang, X.-W. Lou, S-Scheme Co₉S₈@Cd_{0.8}Zn_{0.2}S-DETA hierarchical nanocages bearing organic CO₂ activators for photocatalytic syngas production, Adv. Energy Mater. 13 (2023) 2203290.
- [41] I.-S. Kim, S.-Y. Jang, T. Park, C. Jo, D.-Y. Kim, D.-K. Ko, Femtosecond transient absorption dynamics in low bandgap polymer solar cell materials including poly

- (thienylenevinylene) derivative and benzothiadiazole moiety, Chem. Phys. 461 (2015) 29-33.
- [42] B.-S. Rolczynski, J.-M. Szarko, H.-J. Son, Y.-Y. Liang, L.-P. Yu, L.-X. Chen, Ultrafast intramolecular exciton splitting dynamics in isolated low-band-gap polymers and their implications in photovoltaic materials design, J. Am. Chem. Soc. 134 (2012) 4142–4152.
- [43] E.-N. Powers-Riggs, X. Zuo, M.-R. Young, R.-M. Wasielewski, Symmetry-breaking charge separation in a nanoscale terrylenediimide guanine-quadruplex assembly, J. Am. Chem. Soc. 141 (2019) 17512–17521.
- [44] H.-Y. Zhang, Y.-P. Chen, R. Lu, R.-Y. Li, A.-C. Yu, Charge carrier kinetics of carbon nitride colloid: a femtosecond transient absorption spectroscopy study, Phys. Chem. Chem. Phys. 18 (2016) 14904–14911.
- [45] T.-L. Bahers, C. Adamo, I. Ciofini, A qualitative index of spatial extent in charge-transfer excitations, J. Chem. Theory Comput. 7 (2011) 2498–2506.
- [46] W.-S. Zheng, Z.-J. Zhu, R. Sha, S.-C. Tu, H.-W. Huang, Layered oxyiodide CdBiO₂I: An efficient visible light responsive and scalable photocatalyst, J. Materiomics 11 (2025) 100928
- [47] H. Cai, F. Chen, C. Hu, W.-Y. Ge, T. Li, X.-L. Zhang, H.-W. Huang, Oxygen vacancies mediated ultrathin Bi40₅Br₂ nanosheets for efficient piezocatalytic peroxide hydrogen generation in pure water, Chin. J. Catal. 57 (2024) 123–132.
- [48] Y.-H. Wang, W.-Y. Yu, C.-Y. Wang, F. Chen, T.-Y. Ma, H.-W. Huang, Defects in photoreduction reactions: Fundamentals, classification, and catalytic energy conversion, eScience 4 (2024) 100228.

- [49] S.-N. Li, G.-H. Dong, R. Hailili, L.-P. Yang, Y.-G. Li, F. Wang, Y.-B. Zeng, C.-Y. Wang, Effective photocatalytic H₂O₂ production under visible light irradiation at g-C₃N₄ modulated by carbon vacancies, Appl. Catal. B Environ. 190 (2016) 26–35.
- [50] Y. Xie, Y.-X. Li, Z.-H. Huang, J.-Y. Zhang, X.-F. Jia, X.-S. Wang, J.-H. Ye, Two types of cooperative nitrogen vacancies in polymeric carbon nitride for efficient solardriven H₂O₂ evolution, Appl. Catal. B Environ. 265 (2020) 118581.
- [51] Z.-Y. Teng, W.-A. Cai, W.-W. Sim, Q.-T. Zhang, C.-Y. Wang, C.-L. Su, T. Ohno, Photoexcited single metal atom catalysts for heterogeneous photocatalytic H₂O₂ production: pragmatic guidelines for predicting charge separation, Appl. Catal. B Environ. 282 (2021) 119589.
- [52] H. Yang, B. Xu, Q.-T. Zhang, S.-S. Yuan, Z.-P. Zhang, Y.-T. Liu, Z.-D. Nan, M. Zhang, T. Ohno, Boosting visible-light-driven photocatalytic performance of waxberry-like CeO₂ by samarium doping and silver QDs anchoring, Appl. Catal. B Environ. 286 (2021) 119845.
- [53] Z.-Y. Lu, G.-X. Chen, S. Siahrostami, Z.-H. Chen, K. Liu, J. Xie, L. Liao, T. Wu, D.-C. Lin, Y.-Y. Liu, T.-F. Jaramillo, J.-K. Nørskov, Y. Cui, High-efficiency oxygen reduction to hydrogen peroxide catalysed by oxidized carbon materials, Nat. Catal. 1 (2018) 156–162.
- [54] T.-C. Zhuo, Y. Song, G.-L. Zhuang, L.-P. Chang, S. Yao, W. Zhang, Y. Wang, P. Wang, W.-B. Lin, T.-B. Lu, Z.-M. Zhang, H-bond-mediated selectivity control of formate versus CO during CO₂ photoreduction with two cooperative Cu/X sites, J. Am. Chem. Soc. 143 (2021) 6114–6122.
- [55] L.-C. Grabow, M. Mavrikakis, Mechanism of methanol synthesis on Cu through CO₂ and CO hydrogenation, ACS Catal. 1 (2011) 365–384.